Istituto Nazionale di Fisica Nucleare
Sottosezione di Bari

INFN/AE-71/7
8 Giugno 1971

DIRECT DETERMINATION OF ETA-ZERO BRANCHING RATIOS(+). -

L. Guerriero, C. Nicolini, G.A. Salandin, A. Tomasin(x)
Istituto Nazionale di Fisica Nucleare,

B. Kendall, R.E. Lanou Jr., J.T. Massimo, A.M. Shapiro, M. Widgoff
Brown University, Providence, Rhode Island, (USA)(o).

D.S. Barton, B.A. Nelson, R. Rosenson
Laboratory for Nuclear Science, Massachusetts Institute of Technology, Cambridge, Mass. (USA)(o).

SUMMARY. -

This work reports a determination of the decay branching ratios of the eta-zero meson into 2γ, $3\pi^0$, $\pi^0\gamma\gamma$, $\pi^+\pi^-\pi^0$ and $\pi^+\pi^-\gamma$ modes.

The etas were produced at BNL Cosmotron in the reaction $\pi^- p \to n\eta_0$ at 752.5 MeV/c pion momentum, close to the threshold value of the eta zero production.

The experiment was designed to minimize the systematic errors due to separate evaluations of single channel rates by different expe-

---

(+) - Research performed partially at Brookhaven National Laboratory, Upton, N.Y., USA.

(o) - Work supported in part through funds provided by U.S. Atomic Energy Commission.

(x) - Present address: Laboratorio per lo Studio della dinamica delle Grandi Masse, CNR - Venezia - Italy.

riments. The trigger has been obtained from neutron time of flight and all the decay modes have been detected simultaneously in double spark chamber array. The size of the available sample has been limited by the Cosmotron final shut down.

The results indicate an $\eta^0 \to \pi^0\gamma\gamma$ contribution consistent with zero. The branching ratios for the other channels are $\eta^0 \to 2\gamma$: 38.6 ± 5.9%; $\eta^0 \to 3\pi^0$: 28.1 ± 5.7% $\eta^0 \to \pi^+\pi^-\pi^0$: 25.8 ± 7.9%; $\eta^0 \to \pi^+\pi^-\gamma$: 7.4 ± 8.5%.

1. - INTRODUCTION. -

Eta-zero meson produced in the reaction:

$$\pi^- p \to \eta^0 n$$

can be detected measuring the emission angle and the momentum of the associated neutron. An unbiasses extimate of the η^0 decay-branching ratios can be obtained from an η^0 sample selected with this technique.

The cross section for η^0 production in π-p interaction as a function of the incoming pion momentum is shown in Fig. 1. The cross section reaches its maximum at approximately 760 MeV/c, close enough to the production threshold to constrain the associated neutron within a narrow forward cone. This fact allows the measurement of the neutron angle and time of flight with a detector of acceptable size. Fig. 2 shows the correlation between neutron emission angle and its time of flight for η^0 production, at different incoming momenta.

The η^0 sample used in the present experiment has been obtained at 752.5 MeV/c, as best compromize between production cross section and maximum neutron angle.

At this momentum the η^0 production cross section is about 2.6 mbarns. Other reactions with a neutron in the final state are listed in Table I together with their relative cross sections.

It can be seen that the η^0 signal at 752.5 MeV/c is approximately 1/7 of the total background contributions.

The neutron detector can be selective for η^0 productions, when it subtends a narrow angle near the η^0 kinematic limit ($\sim 22^0$) as shown in Fig. 3 where the angular distributions for the neutron in the $\pi^- p \to n\, \eta^0$ reaction and for $\pi^- p \to n\, \pi^0\pi^0$ phase space production are plotted.

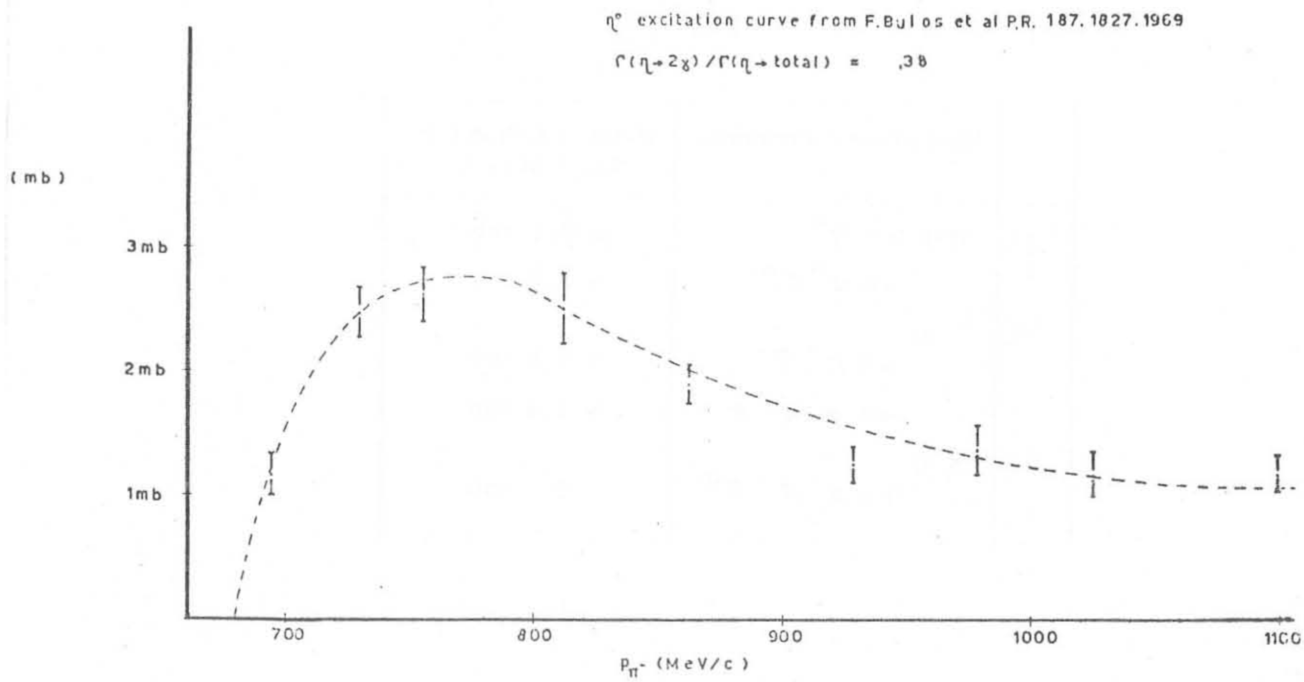

η° excitation curve from F.Bulos et al P.R. 187.1827.1969
Γ(η→2γ)/Γ(η→total) = ,38
(mb)
3mb
2mb
1mb
700
800
900
1000
1100
P_π- (MeV/c)

FIG. 1

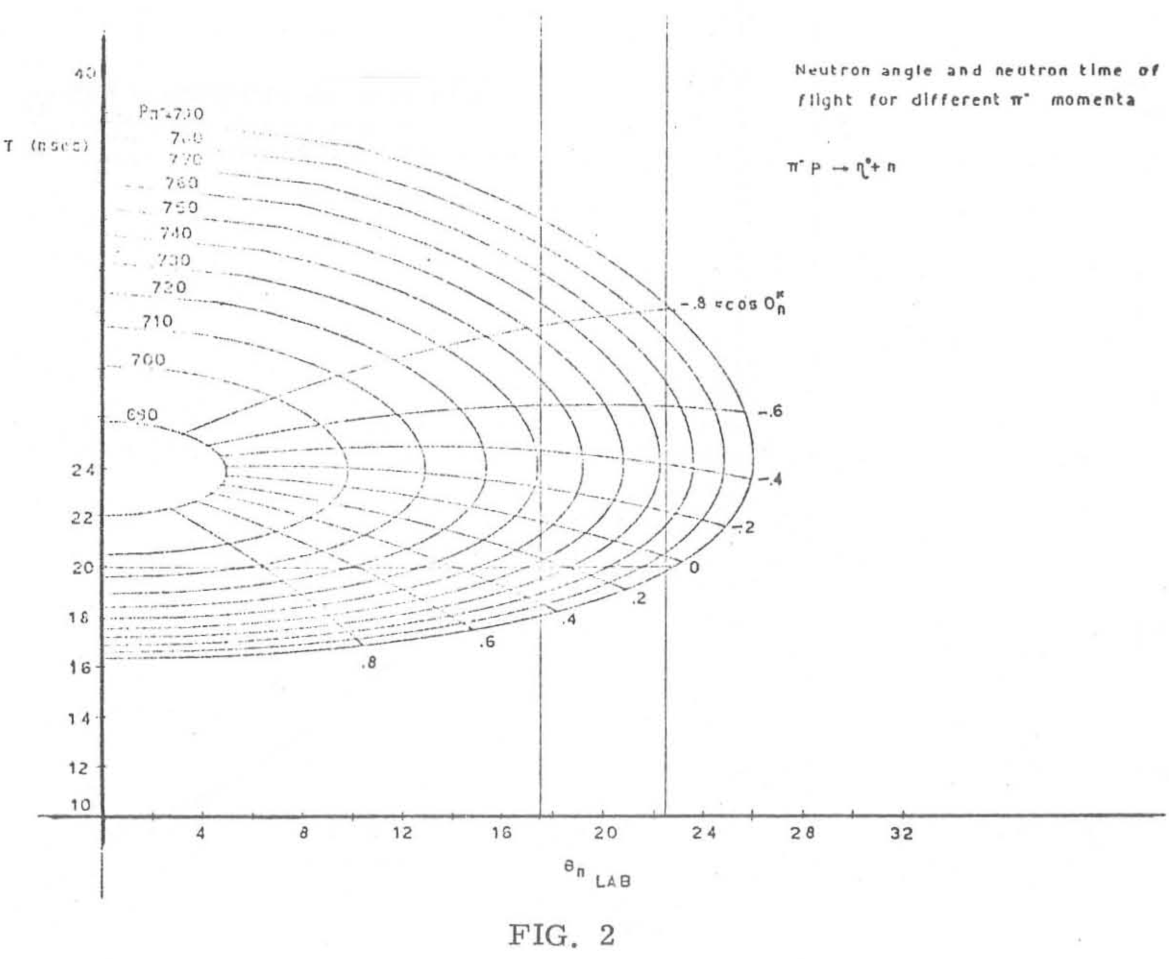

Neutron angle and neutron time of flight for different π⁻ momenta
π⁻ p → η°+ n
T (nsec)
40
24
22
20
18
16
14
12
10
4
8
12
16
20
24
28
32
θn LAB
700
690
-.8 =cos θ*n
-.6
-.4
-.2
0
.2
.4
.6
.8

FIG. 2

TABLE I

	Background channels	Cross sections at 752.5 MeV/c
a)	$\pi^- p \to n\ \eta^0$	$\sim$ 6.5 mb
	$\to n\ \pi^0 \pi^0$	$\sim$ 2.2 mb
b)	$\pi^- p$	
	$\to n\ \pi^+ \pi^-$	$\sim$ 7.0 mb
	$\to n\ \pi^0 \pi^0 \pi^0$	$\sim$ 1.3 mb
c)	$\pi^- p$	
	$\to n\ \pi^+ \pi^- \pi^0$	$\sim$ 2 mb

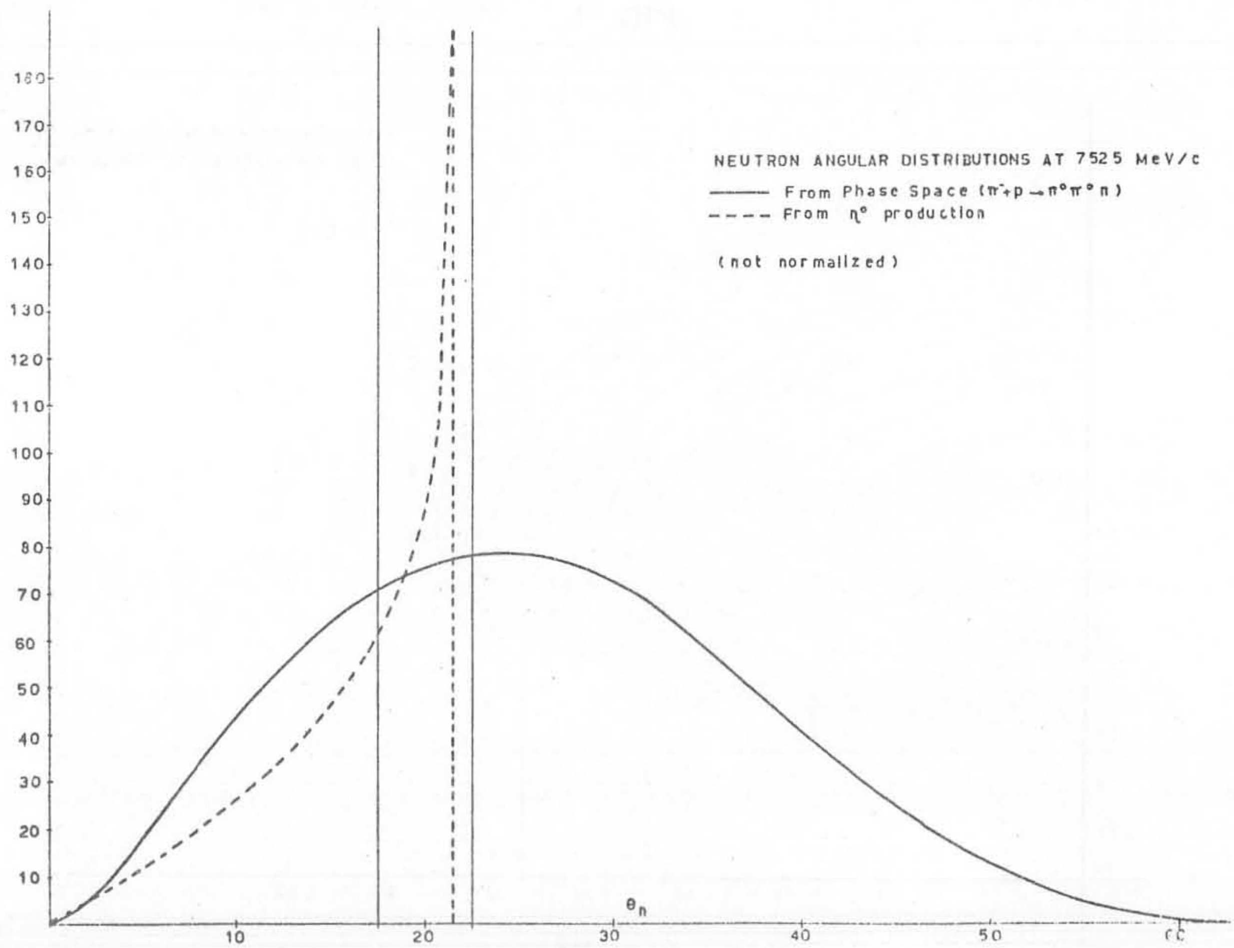

FIG. 3

It can be seen that $\sim 52\%$ of the neutrons from η^0 will appear in 5^0 interval covering the kinematic peack, while only $\sim 16\%$ of the background neutron will go in the same interval. With the neutron detector covering the angle interval $17.4 \div 22.6^0$, the signal to background ratio will be enhanced from $1 \div 7$ to about $1 \div 2$.

Further enchancement of the η^0 signal can be obtained from convenient cuts in the invariant mass of the system of particles accompanying the neutron in the final state. Fig. 4 shows the correlation between the neutron emission angle and neutron time of flight for different values of the invariant mass of the other particles in the final state. The correlation has been evaluated at 752.5 MeV/c incoming pion momentum. Fig. 5 shows the invariant mass distribution for two pions produced according to phase space with the neutron within the selected angular region. The dotted line is the MC prediction for the invariant mass from neutrons produced with η^0's, taking account the experimental errors in the time of flight and angle determination.

With a proper choice for an invariant mass cut, it is possible to eliminate a large fraction of the background, still mantaining the signal almost unreduced.

The final analysis has been performed with an invariant mass cut at 540 MeV corresponding approximately to 1.85 : 1 signal + background/background ratio.

2. - EXPERIMENTAL APPARATUS. -

The experimental apparatus consisted of a small hydrogen target surrounded by a spark chamber array: four large steel chambers to detected electron showers and four small thin foils chambers to detect charged decay products. Three meters distant from the target, at 20^0 with respect to the beam, was a neutron hodoscope, to select the neutron from the eta production reaction by measuring emission angle and time of flight. It subtended approximatly 5.2 degrees of polar angle 1/13 of the total azimuth.

2.1. - Beam transport. -

The circulating beam of the Cosmotron was extracted and then focussed at 3 GeV/c upon a copper target placed between the polefaces of bending magnet B_1 (Fig. 6). The negative particles, focussed by the quadrupoles Q_1-Q_2, were momentum selected by the bending magnet B_2.

Pitching magnets P_1-P_2 were placed to raise the beam 38 inches above the plane of the internal proton beam of the Cosmotron.

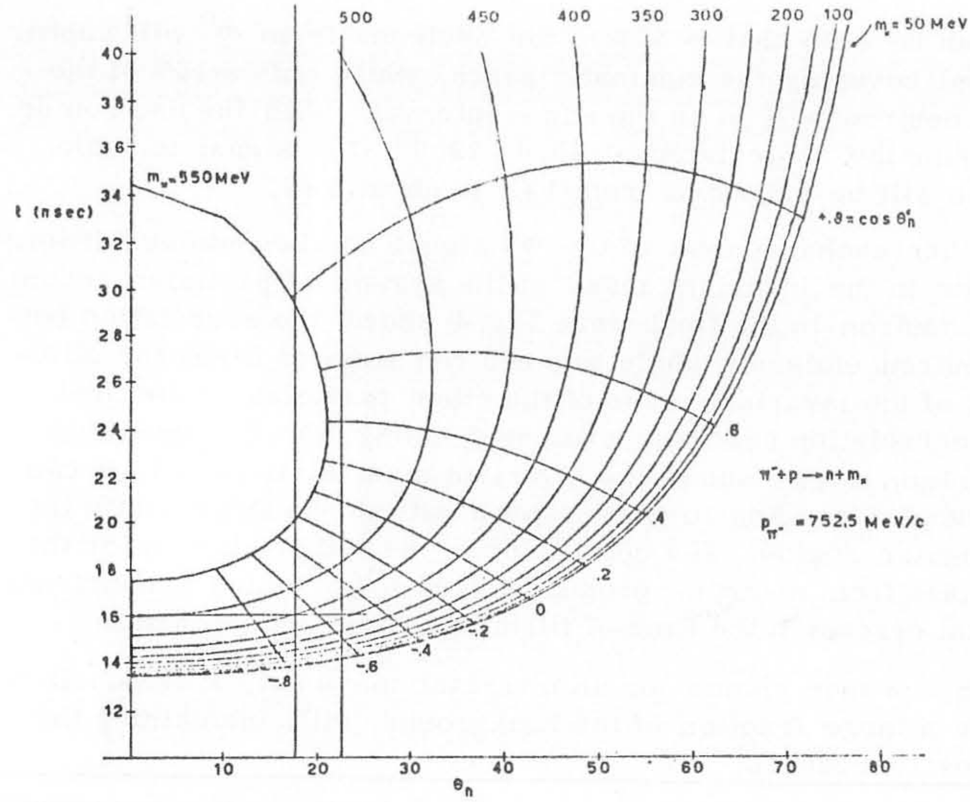

500
450
400
350
300
200
100
m_x = 50 MeV
m_x = 550MeV
t (nsec)
+.8 = cos θ'n
.8
.4
.2
0
-.2
-.4
-.6
-.8
π⁻+p → n+mₓ
p_{π^-} = 752,5 MeV/c
θn

FIG. 4

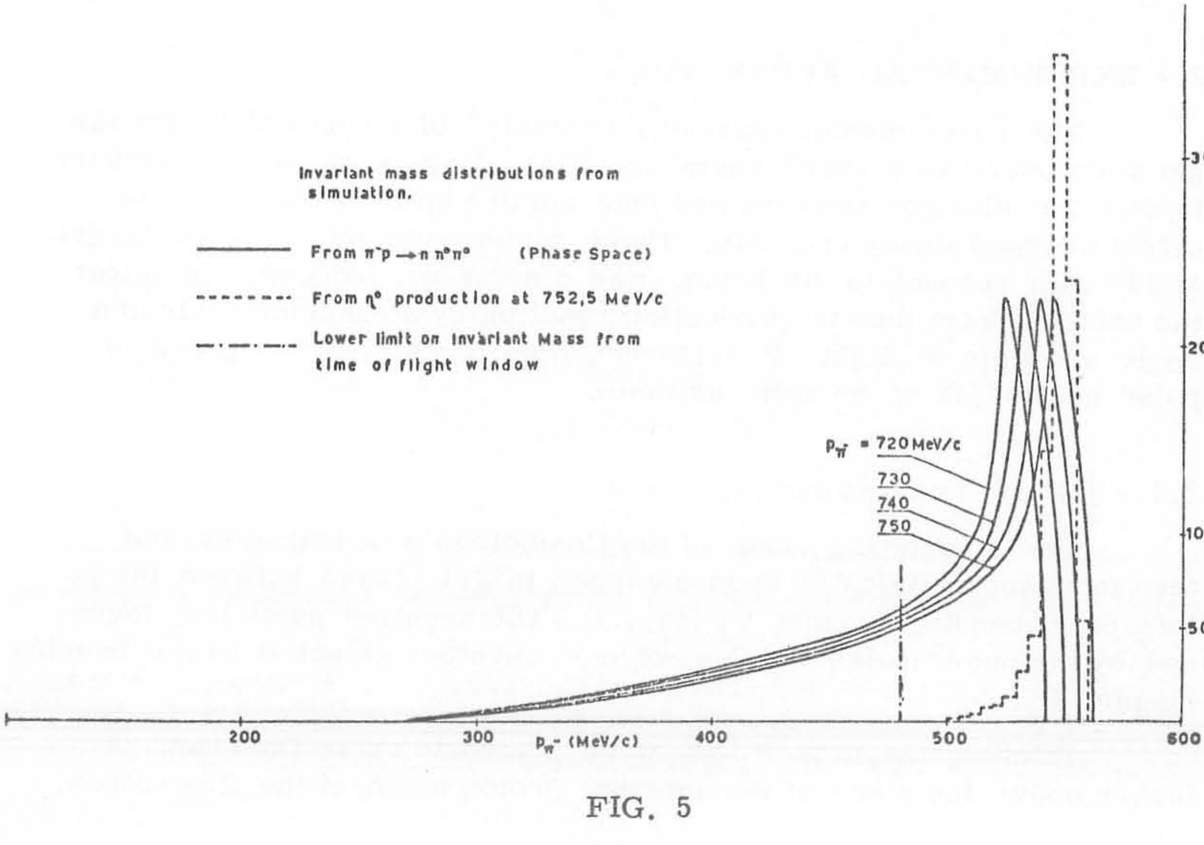

Invariant mass distributions from simulation.
From π⁻p → n π°π° (Phase Space)
From η° production at 752,5 MeV/c
Lower limit on invariant Mass from time of flight window
p_{π^-} = 720 MeV/c
730
740
750
p_{π^-} (MeV/c)

FIG. 5

In this way the chance of spurious interactions in our apparatus has been reduced.

The beam momentum has been determined measuring the central value of the magnetic field in the momentum selecting magnet with a calibrated Hall probe. The momentum loss introduced by counters and thin foil spark chambers preceding the target resulted to be 10.5 MeV/c.

The momentum values have been checked through the CM opening angle distributions of the two gamma decay of the η^0 and of the charge exchange π^0.

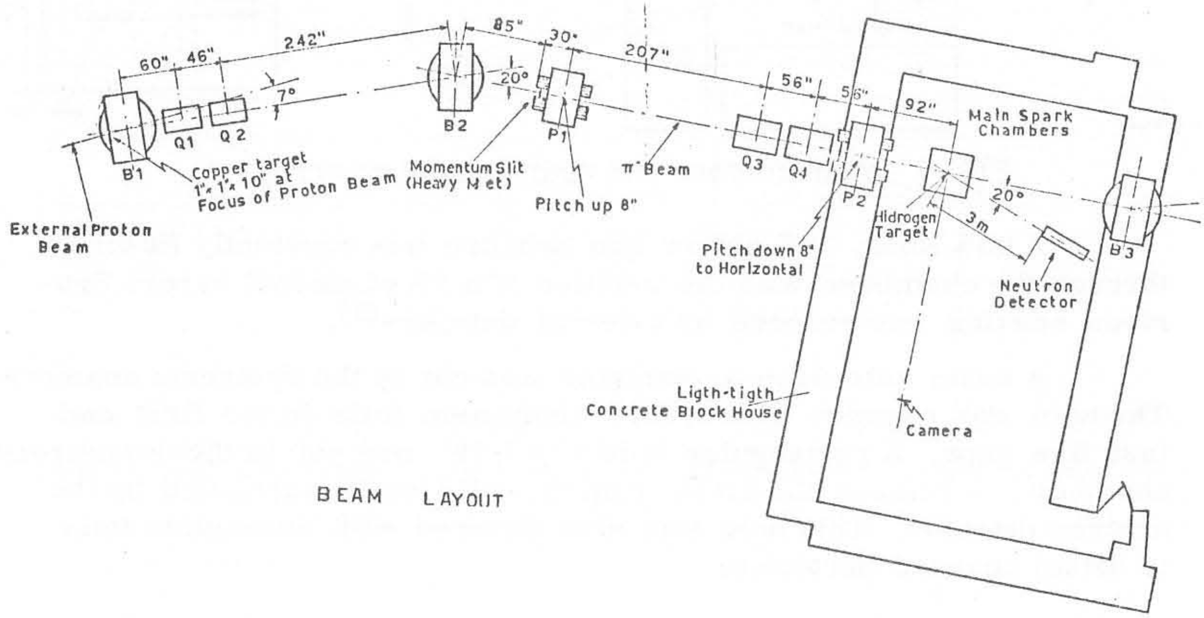

FIG. 6

2.2. - Target. -

The liquid hydrogen target consisted of a spherical Mylar ball, 4 cm in diameter and 0.002 inches wall thickness. The target was surrounded by a Mylar vacuum jacket and mounted on a aluminium frame to which the small thin-foil spark chamber were attached.

2.3. - Spark-chambers. -

The main spark chambers surrounding the target (Fig. 7) were made of fifty one steel plates, 75 cm x 75 cm x 2 mm with 3 mm gaps between the plates. This array provides a total of 5.5 radiation lenght of steel in the direction perpendicular to the plates, ensuring that virtually all photons passing through the chambers were converted to electron-positron showers. The low energy cut off for γ-ray detection in the system has been evaluated at 35 MeV. To detect low energy charged particles and to determine accurately their origins, four small chambers were arrayed close to the target. These chambers were made of five .001'' aluminium foils stretched and glued over 12''x 7''x 1/16'' aluminium frames.

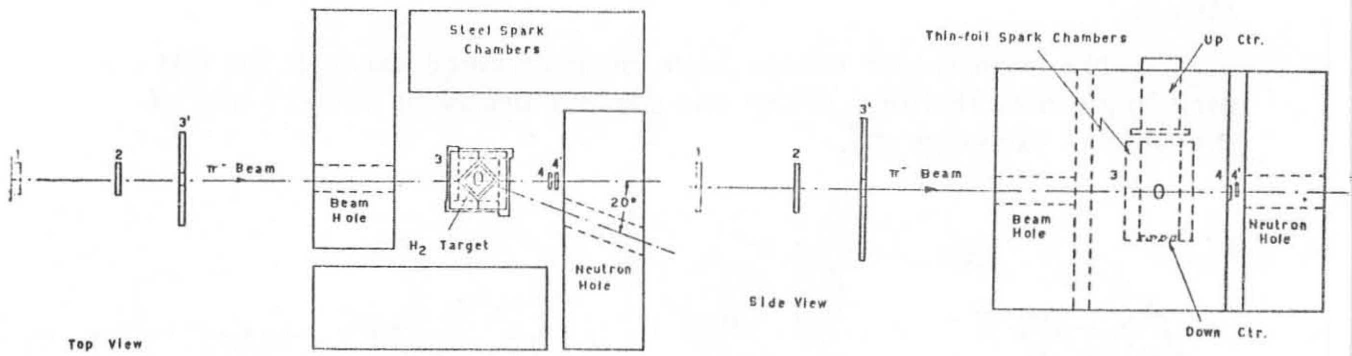

FIG. 7 - Main counter and spark chamber array.

A 90% Neon, 10% helium gas mixture was constantly flowing through the chambers with the addition of a 5% of alcohol vapor. Spurious spaking was reduced by external dampers(1).

A beam hole 9 cm in diameter was cut in the upstream chamber. The hole was covered with 0.001'' aluminium foils in the first and last five gaps. A rectangular hole 4''x 3.75'' was cut in the downstream chamber to remove the steel from the solid angle subtended by the neutron detector. This hole was also covered with aluminium foils to detect charged particles.

2.4.- Neutron detector.-

The neutron detector shown in Fig. 8 consisted of 21 scintillation counters (26 cm x 45 cm x 2.5 cm) alternated with two gaps 0.001'' aluminium foil spark chambers. The charged particles coming from neutron interactions were detected requiring coincidences between any pair of adjacent counters and were observed in the corresponding spark chambers. In order to improve the time resolution of the spark chambers, electrolumiscent panels were attached at the location of each scintillator. Panels corresponding to counters giving pulses in coincidence with the trigger signal were illuminated, to show in the pictures which counters have been triggered by the charged prongs.

The neutron detectors was shilded by an array of anticoincidence counters.

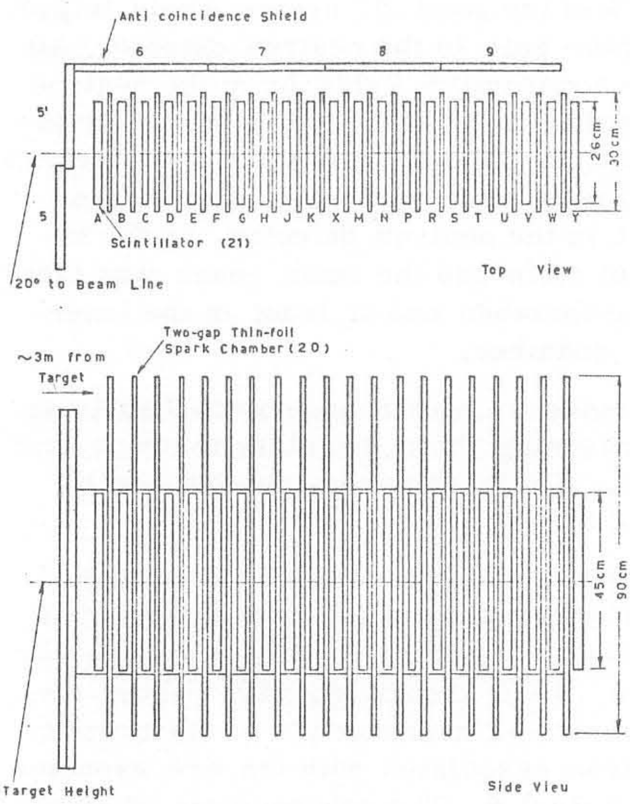

FIG. 8 - Neutron detector array.

2.5. - Counter logic. -

The counter layout for the trigger logic is shown in Fig. 7. Counters 1, 2, 3', 3, define the beam. Counter 3', with a beam defining hole 4 cm in diameter, was used in anticoincidence to eliminate off axis beam particles and charged products from upstream interactions. Two downstream anti-counters 4 and 4', were used as high efficiency veto for noninteracting beam particles.

The neutron detector logic requires a coincidence between at least one pair of adjacent counters in the neutron detector in anticoincidence with counters 5 - 5'.

A good event trigger was generated by a coincidence between one pulse from the telescope 1 2 3' 3 4 4', and one pulse from the neutron detector logic; the telescope pulse was stretched to 48 nsec corresponding to the desired range of the neutron time of flight.

The output of the time to pulse-height converter was digitized in 8 binary-bits and the resulting number, displayed on indicator lights, appeared in the correspondent spark chamber picture.

3. - DATA ACQUISITION. -

The sample has been obtained from 70.000 pictures at 752.5 MeV/c. In addition 8.000 pictures at 721.5 MeV/c, 3.000 pictures at 729.5 MeV/c and 27.000 pictures at 737.5 MeV/c have been used to obtain information on the background since at these momenta the kinematic limit of the neutron angle from η^0 production is lower than the minimum angle subtended by the neutron detector.

Several cuts were made in the scanning table to eliminate background events and speed up the scanning procedure. All photograps with neutron time of flight corresponding to $\beta > 0.6$ were by-passed. In addition during preliminary analysis of the data (confirmed by a Monte Carlo study of the recoil proton in the neutron detector)[2], it was found that approximately 90% of the good η^o events would trigger only one or two consecutive counter pair in the neutron detector. All photographs with more than four consecutive lights on in the neutron detector were therefore disregarded. All events remaining after these two cuts were scanned in detail for charged particles and electron showers in the main detector. Events were measured when a good neutron recoil trach was present in the neutron detector, in the region identified by the luminescent strip and the beam reack was clearly visible in the upstreams large chamber and at least in the innermost gap of the upstream small chamber.

All spark structures accepted as electron showers had to satisfy minimum requirements concerning their direction in space and number of sparks per unit lenght. These requirements introduced an effective low energy cut off of 35 MeV.

During the analysis of the data, it was noticed that a large fraction of events with a charged particle in or close to the hole cut in the steel plates of the downstream chamber, or with a gamma ray which converted close to the hole, were associated with a short time of flight ($\beta > 0.6$). With an error of ~ 2 nanoseconds on the neutron time-of-flight, 99.8% of all neutron associated with eta are expected to appear with beta in the range $0.3 \div 0.6$. The enhancement of high beta events seems be due to negative pions and γ-rays produced on the edge of the solid angle subtended by the neutron detector. These particles may interact in front of the neutron detector anticounters and produce fast neutrons or soft gammas.

The effect can be reduced removing from the sample all events with charged particles and/or showers visible in the 2cm region surrounding the neutron hole.

In addition, to reduce the effect of efficiency variations in the thin foil-chambers, charged particles were required to produce at least one spark in the first gap of large chamber in addition to one or more sparks in the small chambers. These criteria introduced an effective low energy cut-off of ~ 45 MeV on the charged particles from η^o-decay.

Coordinate measurements were done with a precision of about 10 μm on the film. The overall error, due mainly to the reconstruction parameters, is about 2.5 mm in space. The neutron production angle has been determined with an error smaller than 0.5 degrees.

4. - MONTE CARLO EVENTS SIMULATION. -

The general purpose simulation program NVERTEX[(3)] was used to evaluate the detection efficiency for different η-decay modes and to take into account the measuring and reconstruction errors.

Detection efficiency is less than unity since the spark chambers covered only two third of the solid angle surrounding the target. In addition final state particles can be lost as a consequence of the low energy cut-off on gammas and charged particles. Different final states are not expected to appear with equal detection efficiency because of possible triggering of anticounters by gammas or charged particles, while spurious triggers can derive from γ-ray interactions in the N. D.

For the event simulation the angular distribution of the η^0 was assumed to be isotropic in the production center of mass. The Monte Carlo events were also thrown with the assumption of constant matrix elements for the decays. Within statistics, other matrix elements gave indistinguishible results. In order to determine the probability that a given decay mode of the eta zero meson will appear with a topology of i-gammas and j-charged particles in the fiducial volume, the cuts extimated for the experimental sample were applied also to the simulated data.

The probabilities evaluated at 752.5 MeV/c, for an invariant mass cut of 540 MeV, are shown in Table II, together with the detection efficiencies for N π^0 π^0 background reaction generated according to phase space.

5. - NEUTRON TIME OF FLIGHT. -

In order to evaluate the neutron time of flight it was necessary to determine which counters pair in the N. D. sent the first pulse into the time-to-pulse height converter.

TABLE II

Monte Carlo detection - Probabilities at 752.5 MeV/c

Topology decay mode	0γ OC	1γ OC	2γ OC	3γ OC	4γ OC	5γ OC	6γ OC	0γ 1C	1γ 1C	2γ 1C	0γ 2C	1γ 2C	2γ 2C
$\eta \to 2\gamma$	0.0087 $\pm$0.005	.362 $\pm$.012	.462 $\pm$.014	-- --	-- --	-- --	-- --	-- --	-- --	-- --	-- --	-- --	-- --
$\eta \to \pi^0\gamma\gamma$	0.007 $\pm$.001	0.101 $\pm$ .003	.287 $\pm$.006	.340 $\pm$.006	.141 $\pm$.004	-- --	-- --	-- --	-- --	-- --	-- --	-- --	-- --
$\eta \to 3\pi^0$	.0009 $\pm$.0002	.0015 $\pm$.0011	.0923 $\pm$.0031	.260 $\pm$.006	.278 $\pm$.006	.165 $\pm$.004	.0361 $\pm$.0018	-- --	-- --	-- --	-- --	-- --	-- --
$\eta \to \pi^+\pi^-\pi^0$	.0006 $\pm$.0003	.008 $\pm$.002	.010 $\pm$.002	-- --	-- --	-- --	-- --	.024 $\pm$.002	.0162 $\pm$.006	.108 $\pm$.005	.063 $\pm$.004	.243 $\pm$.008	.162 $\pm$.006
$\eta \to \pi^+\pi^-\gamma$	.004 $\pm$.001	.018 $\pm$.002	-- --	-- --	-- --	-- --	-- --	.111 $\pm$.005	.194 $\pm$.007	-- --	.182 $\pm$.007	.305 $\pm$.005	-- --
$\pi^0\pi^0$	.002 $\pm$.001	.020 $\pm$.004	.051 $\pm$.002	.056 $\pm$.008	.020 $\pm$.004	-- --	-- --	-- --	-- --	-- --	-- --	-- --	-- --

The time-of-flight of a neutron from the target to its interaction point is related to the A/D time by the following equation:

$$T_{A/D} = T_N + T_L^{(i)} + T_o^{(i)} + T_R^{(i)} = T_N + T(i)$$

where $T_{A/D}$ = time shown in the A/D lights;

T_N = time of flight of the neutron;

$T_L^{(i)}$ = the time taken by the light to travel from the point of emission in the i^{th} scintillator to the photomultiplier. (The effective index of refraction has been measured and its value is n = 2.4)[4];

$T_o^{(i)}$ = a correction term characteristic of counter pair i, i+1, to compensate intrinsic delay of photomultipliers, circuits and cables;

$T_R^{(i)}$ = time of flight of the recoil proton to reach the i^{th} counter, as calculated from the residual range of the proton in the scintillator.

To resolve the ambiguity as to which counter pair gave timing signal, we have to find the earliest signal from the different counter pair i triggered by the recoil charged particle. This will be given from the i pair for which T(i) is minimum.

The time constant $T_o^{(i)}$ were determined by calibration with elastic scattering events: 5.000 pictures have been taken triggering the neutron detector, pair by pair, on elastic scattering. These measurements gave a time spread of about 2 nanoseconds.

6. - BACKGROUND EVALUATION. -

The η^o sample has been obtained at 752.5 MeV/c π^- incident momentum. At this energy, relevant contributions can derive from the following background reactions

$$\pi^- p \to \pi^o n; \qquad \pi^- p \begin{cases} \to n\,\pi^+\pi^- \\ \to n\,\pi^o\pi^o \end{cases}; \qquad \pi^- p \begin{cases} \to n\,\pi^o\pi^o\pi^o \\ \to n\,\pi^+\pi^-\pi^o \end{cases}$$

Charge exchange contributions can easily be eliminated with the invariant mass cut.

The remaining background is excepted to derive mainly from two pions final states, since the phase space available for three pions final states is very limited.

Background contributions to each topology have been evaluated on samples produced at lower beam momenta, having the neutron detector outside the kinematic limit for the neutron associated to the η^o. For this reason data have been taken at 721.5, 729.5 and 737.5 MeV/c. At this last momentum, η^o events can send the neutron in the inner half of the neutron detector ($\theta_N < 19^o$). Therefore, for this sample, only events with $20^o < \theta_N < 22.6^o$ have been considered for the background evaluation.

Table III shows the number of events observed with different topologies for the background and the signal sample together with the relative number of incident pions. It can be noticed that the limited variations in the beam momentum do not appear to affect, within statistics, the partition of background events among the different channels. The background contribution at 752.5 MeV/c can therefore be obtained normalizing properly the data at lower momenta.

TABELLA III

Topologies	Invariant Mass cut = 110 MeV/c^2 $\theta_N < 22^o$			
N^o of pions	0.502×10^9	0.0086×10^9	0.550×10^9	3.124×10^9
Momentum MeV/c	721.5	727.5	737.5	752.5
0 γ 0C	7	2	8	85
1 γ 0C	22	7	29	287
2 γ 0C	44	15	58	527
3 γ 0C	27	6	18	189
4 γ 0C	7	1	20	108
5 γ 0C	4	1	4	58
6 γ 0C	1	0	0	22
0 γ 1C	56	13	54	460
1 γ 1C	14	1	15	137
2 γ IC	9	1	11	63
0 γ 2C	75	13	74	525
1 γ 2C	5	2	14	132
2 γ 2C	2	1	6	58
Total	273	63	311	2651

The invariant mass distributions for signal and background events have been taken into account, to minimize subtraction uncertainties.

As discussed in par. 1 if only events corresponding to an invariant mass greater than 540 MeV are considered, the signal should be reduced by 10%, while almost two thirds of the background is removed (see Fig. 10).

Fig. 9 shows the invariant mass distribution for the background events at 721.5 MeV/c evaluated from neutron angle and time of flight.

Fig. 5 shows the invariant mass distributions predicted for $n \pi^0 \pi^0$ final states produced according to phase space. It can be seen that the kinematic limit varies appreciably with the incoming momentum.

In order to subtract the background events channel by channel, equivalent cuts have to be applied to the different samples. These cuts correspond to appropriate invariant mass values which can be evaluated requiring at each momentum the inclusion of the same fraction of the invariant mass distribution for phase space generated events.

Equivalent cut values are given in Table IV.

TABLE IV

INCOMING MOMENTUM	752.5	737.5	729.5	721.5
	540	535	530	525
INVARIANT	530	526	521	517
MASS (MeV)	520	519	515	510
CUTS	500	500	495	490

With these cuts at the different beam momenta, each incoming pion has the same probability to produce a background event in the accepted region of invariant mass, and normalizations of different samples can be done simply on the numbers of incoming pions.

Table V shows the events observed with different topology at 752.5 MeV/c, at different invariant mass cuts, together with the backgrounds.

Table VI shows the (Signal + Background)/Background ratios, for each observed topology and for different invariant mass cuts.

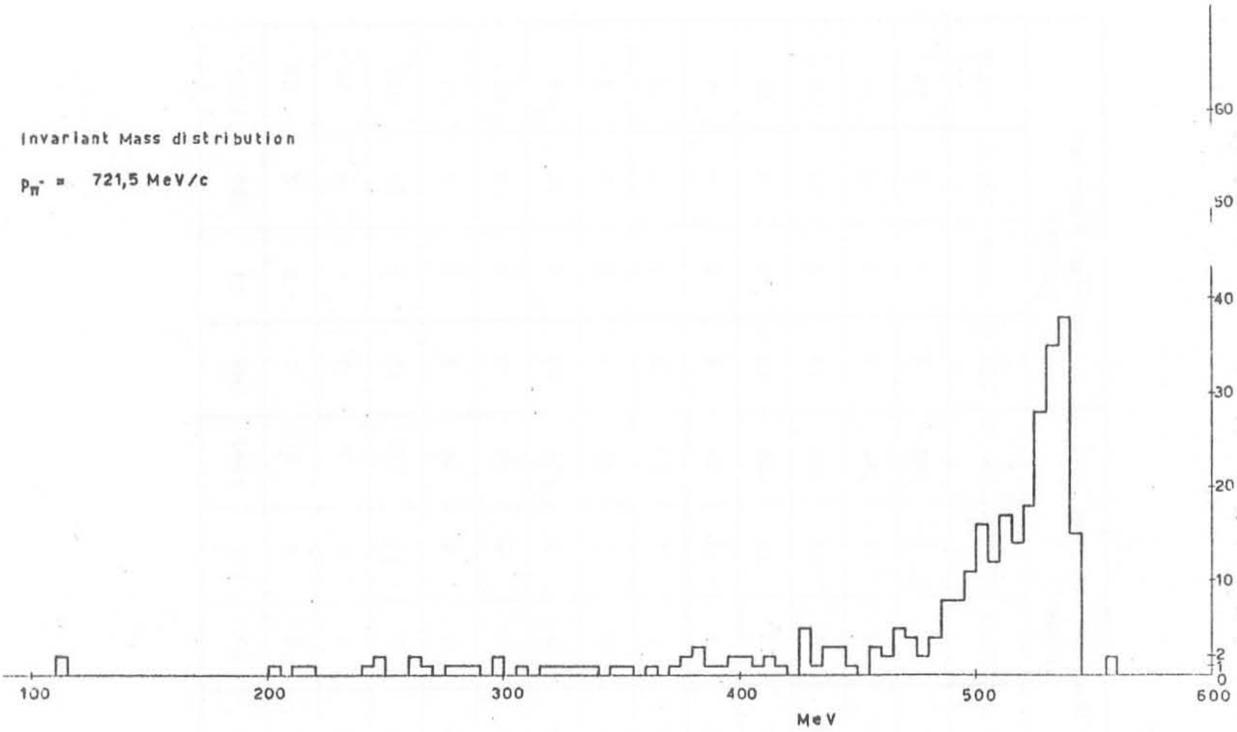
Invariant Mass distribution
p_{π^-} = 721,5 MeV/c
MeV

FIG. 9

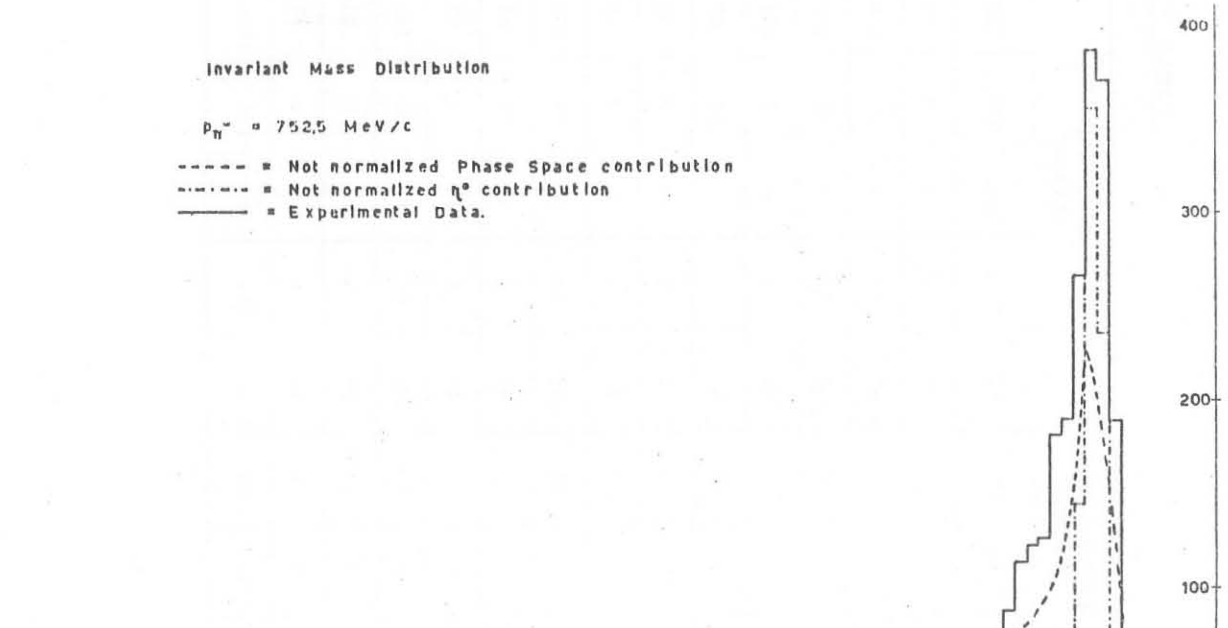
Invariant Mass Distribution
p_{π^-} = 752,5 MeV/c
----- = Not normalized Phase Space contribution
-·-·-·- = Not normalized η^0 contribution
——— = Experimental Data.
MeV

FIG. 10

TABLE V

Topologies	Invariant Mass cut 500 MeV				Invariant Mass cut 520 MeV				Invariant Mass cut 530 MeV				Invariant Mass cut 540 MeV			
Momentum MeV/c	721.5	729.5	737.5	752.5	721.5	729.5	737.5	752.5	721.5	729.5	737.5	752.5	721.5	729.5	737.5	752.5
0 γ 0C	4	1	4	69	1	1	4	55	1	1	4	48	1	0	2	38
1 γ 0C	12	5	21	187	11	4	17	158	7	3	13	131	6	0	9	102
2 γ 0C	22	9	42	345	21	6	35	289	18	4	29	260	16	3	21	210
3 γ 0C	19	3	15	143	15	3	12	121	13	3	10	108	10	2	7	81
4 γ 0C	6	1	18	91	5	1	15	87	5	1	10	79	4	0	7	75
5 γ 0C	3	1	4	53	2	1	3	50	2	1	3	47	2	1	2	36
6 γ 0C	1	0	0	21	1	0	0	21	1	0	0	20	1	0	0	18
0 γ 1C	44	5	38	327	33	3	31	274	27	3	27	234	23	3	18	175
1 γ 1C	8	1	12	102	6	0	10	86	5	0	9	75	5	0	6	62
2 γ 1C	6	0	9	46	5	0	8	42	4	0	4	34	2	0	2	27
0 γ 2C	65	9	60	405	48	8	50	341	41	7	43	302	31	4	33	217
1 γ 2C	5	2	11	110	5	2	8	95	4	2	6	75	3	1	5	58
2 γ 2C	2	0	6	44	1	0	5	39	1	0	4	35	1	0	3	33
Total	197	37	242	1943	154	29	198	1658	129	25	162	1448	106	14	115	1132

TABLE VI

Cuts	total S/B	0γ 0C	1γ 0C	2γ 0C	3γ 0C	4γ 0C	5γ 0C	6γ 0C	0γ 1C	1γ 1C	2γ 1C	0γ 2C	1γ 2C	2γ 2C
110 MeV/c^2 $\theta_N < 22^o$	1.52	1.85	1.83	1.67	1.37	1.44	2.38	8.1	1.40	1.65	1.11	1.2	2.32	2.39
500 MeV/c^2 $\theta_N < 22^o$	1.52	2.84	1.82	1.75	1.44	1.35	2.45	7.8	1.40	1.80	1.14	1.12	2.26	2.04
520 MeV/c^2 $\theta_N < 22^o$	1.64	3.39	1.83	1.73	1.49	1.47	3.08	7.8	1.52	1.98	1.20	1.21	2.34	3.41
530 MeV/c^2 $\theta_N < 22^o$	1.70	2.96	2.11	1.89	1.54	1.79	2.89	7.4	1.52	1.97	1.57	1.23	2.32	2.6
540 MeV/c^2 $\theta_N < 22^o$	1.85	4.7	2.52	1.95	1.58	2.52	2.67	6.7	1.48	2.09	2.5	1.18	2.39	3.06

The ratios show significant improvements for increasing missing mass cuts as expected from kinematic and geometric consideration (see par. 1). A separate analysis on single channels shows a reasonable agreement with Monte Carlo prediction, also for the topologies 0γ 1C, 0γ 2C and 3γ 0C. In these channels two simultaneous effect contribute to keep low signal/noise ratio, even increasing the missing mass cuts: the large contributions of background reactions as

$$\pi^- p \to n \pi^+ \pi^- ; \qquad \pi^- p \to n \pi^o \pi^o$$

and the small contribution of the η_o decays to these topologies. The numbers of events at 540 MeV cut, after subtraction of the normalized background, have been fitted to obtain the η^o branching ratios.

7. - FIT. -

The final event sample after background subtraction is given in Table VII. For each topology the corrected number of η^o events is given, together with the statistical error.

With the experimental data and the detection efficiency obtained from the simulation, the following equation can be written:

$$\sum_{1}^{5}{}_k \, a_{ik} N_k = n_i \qquad (i = 1, 13)$$

where

n_i = number of events for the i-topology

N_K = number of η_o parents decaying in the K mode

a_{ik} = M.C. probability.

TABLE VII

Topologies	Signal + Background	Normalized Background	Subtracted Sample
0γ 0C	38 ± 6.1	8.1 ± 4.6	29.9 ± 7.6
1γ 0C	102 ± 10.1	40.5 ± 10.5	61.5 ± 14.5
2γ 0C	210 ± 14.5	108. ± 17.0	102. ± 22.3
3γ 0C	81 ± 9.0	51.3 ± 11.7	29.7 ± 14.8
4γ 0C	75 ± 8.6	29.7 ± 8.9	35.3 ± 12.4
5γ 0C	36 ± 6.0	13.5 ± 6.0	22.5 ± 8.4
6γ 0C	18 ± 4.2	2.7 ± 2.7	15.3 ± 5.0
0γ 1C	175 ± 13.2	118.8 ± 18.	56.2 ± 22.3
1γ 1C	62 ± 6.3	29.7 ± 8.9	32.3 ± 11.9
2γ 1C	27 ± 5.2	10.8 ± 5.4	16.2 ± 7.5
0γ 2C	217 ± 14.7	183.6 ± 22.2	33.4 ± 26.7
1γ 2C	58 ± 7.6	24.3 ± 8.1	33.7 ± 11.0
2γ 2C	33 ± 5.7	10.8 ± 5.4	22.2 ± 7.8

To find the best fitted solution for the N_K's, we have to minimize the function

$$\chi^2 = \sum_{1}^{13} {}_i \frac{\left(\sum_{1}^{5} {}_k\, a_{ik} N_k - n_i\right)^2}{\sigma^2_{EXP} + \left(\sum_{1}^{5} {}_k\, \Delta a_{ik} N_k\right)^2}$$

where

Δa_{ik} = M.C. uncertainties on a_{ik}

$\sigma^2_{EXP} = n_{i(SIGNAL)} + f\, n_{i(NORMAL\ BACKGR.)}$

f = normalizing factor.

The MINFUN program[5] has been used to search the best solution. Parameter space has been first explored in searching mode and final fitted values have been obtained running the program in converging mode.

8. - CONCLUSIONS. -

a) All topologies included
13 equations with 5 unknown
$\chi^2 = 13.4$

Decay mode	Fitted number of parents
2γ	201.6 ± 31.6
$\pi^o\gamma\gamma$	-37.6 ± 41.2
$3\pi^o$	173.1 ± 47.5
$\pi^+\pi^-\pi^o$	127.6 ± 39.0
$\pi^+\pi^-\gamma$	35.8 ± 42.8

VARIANCE MATRIX

0.1001D 04	-0.5022D 03	0.3881D 03	0.8690D 01	-0.3658D 02
-0.5022D 03	0.1702D 04	-0.1574D 04	-0.6891D 01	0.9897D 01
0.3881D 03	-0.1574D 04	0.2251D 04	0.4127D 01	-0.5827D 01
0.8690D 01	-0.6891D 01	0.4127D 01	0.1521D 04	-0.1191D 04
-0.3658D 02	0.9897D 01	-0.5827D 01	-0.1191D 04	0.1838D 04

The resulting branching ratios are:

BRANCHING RATIOS	
$37.4 \pm 5.8\%$	2γ
$-7.0 \pm 7.6\%$	$\pi^o\gamma\gamma$
$32.1 \pm 8.8\%$	$3\pi^o$
$23.85 \pm 7.2\%$	$\pi^+\pi^-\pi^o$
$6.65 \pm 7.9\%$	$\pi^+\pi^-\gamma$

The $\pi^o\gamma\gamma$ mode seems consistent with 0.

b) Since the $\pi^o\gamma\gamma$ decay mode of the η^o seems consistent with zero, a separate fit has been done without the $\eta^o \rightarrow \pi^o\gamma\gamma$ channel: 13 equations with 4 unknowns $\chi^2 = 14.3$.

Decay mode	Fitted number of parents
2γ	190.6 $\pm$29.2
$3\pi^o$	138.6 $\pm$28.2
$\pi^+\pi^-\pi^o$	127.4 $\pm$39.0
$\pi^+\pi^-\gamma$	36.07$\pm$42.8

VARIANCE MATRIX

0.8532D 03	-0.7634D 02	0.6660D 01	-0.3367D 02
-0.7634D 02	0.7958D 03	-0.2245D 01	0.3326D 01
0.6660D 01	-0.7958D 03	0.1521D 04	-0.1191D 04
-0.3367D 02	0.3326D 01	-0.1191D 04	0.1838D 04

The resulting branching ratios are:

BRANCHING RATIOS

38.6$\pm$5.9%	2γ
28.1$\pm$5.7%	$3\pi^o$
25.8$\pm$7.9%	$\pi^+\pi^-\pi^o$
7.4$\pm$8.5%	$\pi^+\pi^-\gamma$

The fraction of neutral decays of the η^o results $\Gamma(\eta^o \rightarrow \text{neutrals})/ / \Gamma(\eta^o \rightarrow \text{total}) = 0.08$. These ratios are in good agreement with the known world average.

APPENDIX I. -

An integral consistency check can be performed considering the CM opening angle distributions for the 2 γ events. These distributions allow a clean separation of events produced by η^o decay.

On the background samples, we can therefore determine the number of events deriving from 2 π^o and 3 π^o channels and appearing as 2 γ in the opening angle region typical of the η^o.

With the invariant mass cut at 540 MeV and $142 < \theta_{0P} < 180$, the normalized number is:

$$N_{2\pi^o + 3\pi^o} = 21 \pm 6.7$$

In the sample at 752.5 MeV/c, with the same cut in the invariant mass, the number of 2 γ events with $142 < \theta_{0P} < 180$ is:

$$N_{\eta^o + 2\pi^o + 3\pi^o} = 114 \pm 10.7$$

The detector efficiency for both gammas of the η is 0.462 $\pm$ $\pm$ 0.014 (see Table II).

We can therefore evaluate the number of $\eta^o \rightarrow 2\gamma$ in our sample

$$(\eta \rightarrow 2\gamma) = \frac{(114 \pm 10.7) - (21 \pm 6.7)}{0.462 \pm 0.014} = 201 \pm 28$$

in good agreement with the previous estimate.

REFERENCES. -

(1) - L. Guerriero et al., Rev. Sci. Instr. 37, 118 (1966).
(2) - C. Nicolini, Thesis, Padova University (1967).
(3) - C.A. Bordner Jr., A.E. Brenner and E.E. Ronat, Rev. Sci. Instr., 37, 36 (1966).
(4) - Rosenson, Kirkpatrik and Thern: "A measurement of the effective index refraction of scintillator" - M.I.T. Internal Report (1967).
(5) - CERN Program library, D 502 (1965).